1 PERKIN

Synthesis and self-aggregation of zinc chlorophylls possessing an ω-hydroxyalkyl group: effect of distance between interactive hydroxy group and chlorin moiety on aggregation †

Shiki Yagai [a] **and Hitoshi Tamiaki** *[a,b]

[a] *Department of Bioscience and Biotechnology, Faculty of Science and Engineering, Ritsumeikan University, Kusatsu, Shiga 525-8577, Japan*
[b] *"Form and Function" PRESTO, Japan Science and Technology Corporation (JST), Kusatsu, Shiga 525-8577, Japan*

Received (in Cambridge, UK) 5th September 2001, Accepted 15th October 2001
First published as an Advance Article on the web 8th November 2001

Zinc 13[1]-oxochlorins **2**, **3** and **3D** possessing 2-hydroxyethyl, 3-hydroxypropyl and 3-hydroxyprop-1-enyl groups, respectively, at the 3-position are synthesized as models for self-aggregative antenna chlorophylls in green photosynthetic bacteria. Self-aggregation of **2**, **3** and **3D** in nonpolar organic solvents and in the solid state is compared with that of **1** possessing a 3-hydroxymethyl group to determine the effect of the distance between the hydroxy group and the chlorin moiety on the self-aggregation. Visible spectral analyses in hexane containing a small amount of THF reveal that the aggregation abilities decrease in the order of **1** ⟶ **2** ⟶ **3**, with an increase of conformational flexibility of the ω-hydroxyalkyl group in a molecule. Aggregated **2** and **3** give absorption maxima at 701 and 702 nm, respectively, red-shifted from the corresponding monomeric absorption (644 nm). These red-shifts are smaller than that of **1** (647 ⟶ 740 nm), which is attributable to the expanded chlorin π–π plane distance in the self-aggregates of **2** and **3**. Furthermore, their CD and IR spectra reveal that the aggregates of **3** are relatively disordered and have weak intermolecular noncovalent interactions among the hydroxy group, central zinc and keto group in the supramolecule. Aggregated **3D** shows a relatively small red-shift of absorption from monomer to aggregates (654 ⟶ 680 nm) due to the decreased overlap between the chlorin π-planes in the aggregated state. However, **3D** easily forms precipitates composed of structurally ordered large aggregates, indicating that **3D** is favorable for molecular packing in the aggregates.

Introduction

Spontaneous molecular self-assembly to construct elaborate supramolecular structures is a scientifically interesting phenomenon.[1] A minimal modulation of building blocks can be amplified in a drastic change of the supramolecular structure through noncovalent interactions. Natural systems offer good examples of sophisticated molecular self-assembly. One of the best examples can be found in the organization of chlorophyllous pigments in extramembranous light-harvesting antenna complexes of green photosynthetic bacteria. In the antenna complex called chlorosome, chlorophyllous pigments self-assemble to function as light-harvesting and energy-transferring devices without structural supports by any proteins,[2,3] while the core of antenna functions of all other photosynthetic organisms such as higher plants and algae is served by chlorophyll(Chl)–protein complexes.[4,5]

The main light-harvesting pigments in the chlorosome are bacteriochlorophyll(BChl)s-*c*, -*d* and -*e* (Fig. 1), which are found exclusively in chlorosomes and are therefore called chlorosomal Chls. The molecular structures of chlorosomal Chls strikingly differ from those of protein-binding Chl-*a* and -*b*; BChl-*c*, -*d* and -*e* possess a 1-hydroxyethyl group at the 3-position instead of the vinyl group that Chls-*a* and -*b* have. It has been established that the hydroxy group of a chlorosomal Chl molecule simultaneously forms a coordinate bond with the central magnesium of the second molecule and a hydrogen bond with the 13-keto group of the third molecule as in C=O ··· H–O ··· Mg, and thereby chlorosomal Chls can construct highly ordered supramolecular self-assemblies[2,6] which are stabilized by π–π interaction between the chlorin macrocyclic π-conjugates.[7] Investigation of molecular–structural specificity of chlorosomal Chls would not only facilitate elucidation of the supramolecular structure of chlorosomal aggregates but also provide insight into the design of building blocks in any synthetic self-assemblies.

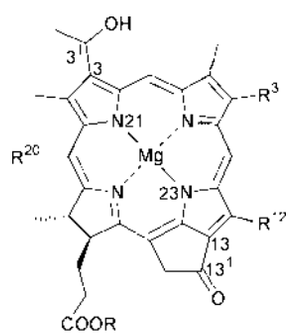

Fig. 1 Molecular structures of naturally occurring chlorosomal chlorophylls.

In the self-assemblies, one of the important factors in the construction of a well-organized supramolecular structure may lie in characteristics of the linker unit attaching the interactive

† Alternative synthetic approach for **12** and **12D** and IR spectra of the precipitates of **3D** are available as supplementary data. For direct electronic access see http://www.rsc.org/suppdata/p1/b1/b107902f

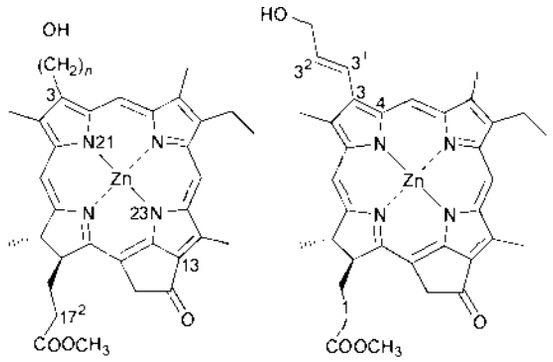

1 (n = 1)
2 (n = 2)
3 (n = 3)

3D

Fig. 2 Synthetic zinc chlorins **1**–**3** and **3D**.

sites in a composition molecule with the building block matrix. This factor can determine the spatial 'intra' supramolecular distance and orientation of building blocks in a supramolecule. In chlorosomal Chls, the hydroxy group, the most important interactive site, is simply attached to the chlorin macrocyclic moiety through one carbon atom (Fig. 1). It is reasonable to assume that coordination of such a hydroxy group to the central magnesium of the adjacent molecule could keep the chlorin molecules very close to each other, accompanied by overlap of the chlorin π-systems. In this situation, these molecules must be stabilized by strong π–π interaction, which leads to formation of large and stable aggregates as well as to strong excitonic interaction among pigments. This leads to a large red-shift of Q_y absorption maxima (≈ 750 nm), which is vital for green bacterial survival in view of efficient energy transfer to the acceptor BChl-*a*; this has a near-infrared absorption band in the baseplate that situates in a chlorosomal membrane and binds to the membranous surface of the cytoplasmic side.[3] Despite the importance of such a methylene linkage, no report has been available on the effect of the linker between the interactive hydroxy group and the chlorin macrocyclic moiety.

Here, we address the extension of C3–C3^1 covalent linkage between the hydroxy group and the chlorin moiety in chlorosomal Chls. Zinc chlorin **1** possessing a hydroxymethyl group at the 3-position is known to be a good model compound for naturally occurring chlorosomal Chls (Fig. 2).[8] Visible absorption, CD and IR spectroscopic properties of self-aggregates of **1** formed in nonpolar organic solvents such as 1% tetrahydrofuran (THF)–hexane are very similar to those of isolated chlorosomal Chls aggregates and the *in vivo* chlorosomal aggregates. Though such spectroscopic similarities generally provide no direct evidence of structural resemblance between their supramolecules, it can be clear that the aggregates of **1** are large and highly ordered as chlorosomal aggregates. Moreover, the aggregates of **1** proved to transfer the excitation energy to an acceptor bacteriochlorin molecule as a functional model of natural chlorosomal antennas.[9–11] We chose zinc chlorin **1** as a natural-type model compound possessing the shortest linker (3-CH_2) between the hydroxy group and the chlorin macrocyclic moiety. We prepared zinc chlorins **2** and **3** possessing a flexible linker (3-CH_2CH_2 and 3-$CH_2CH_2CH_2$, respectively), and **3D**‡ possessing a fairly rigid linker (3-CH=CH–CH_2) by novel synthetic approaches for functionalization of the 3-vinyl and 3-formyl groups of chlorophyll derivatives (Fig. 2). Self-aggregation behavior of zinc chlorins **2**, **3** and **3D** in nonpolar organic solvents was examined and compared with that of **1** to elucidate the importance of the distance between the interactive hydroxy group and the chlorin macrocyclic moiety in chlorosomal Chls.

Results and discussion

Synthesis of the zinc chlorin 2

Synthesis of the 3-(2-hydroxyethyl)chlorin **6** (Scheme 1) has been reported by Smith *et al.*[12] The synthetic route was as follows: treatment of methyl pyropheophorbide-*a* (3^1,3^2-didehydrophytochlorin methyl ester **4D** in Scheme 1) with thallium trinitrate trihydrate ⟶ removal of chelated thallium by sulfur dioxide gas ⟶ acid treatment of the resulting dimethoxyacetal ⟶ reduction of the resulting 3-(formylmethyl)chlorin

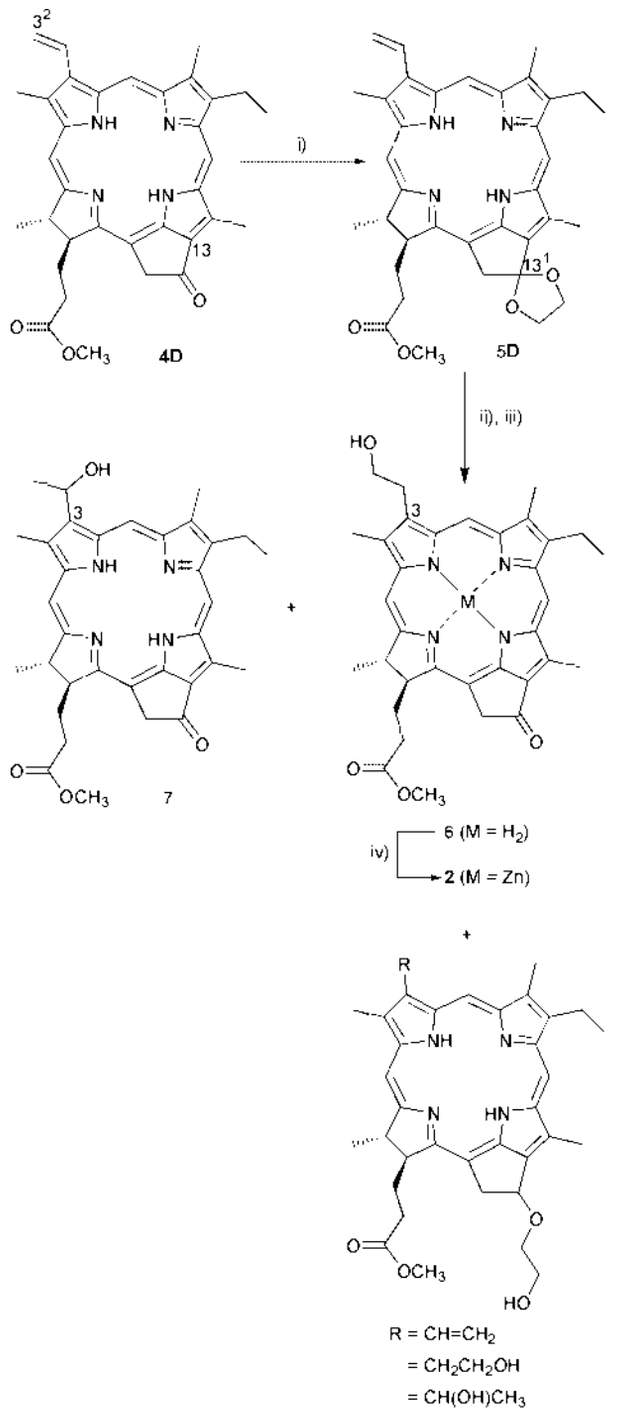

Scheme 1 *Reagents and conditions*: (i) $(CH_2OH)_2$–$(CH_3)_3SiCl$, dry CH_2Cl_2; (ii) BH_3–THF, then H_2O_2–NaOH; (iii) aq. HCl–acetone; (iv) $Zn(OAc)_2 \cdot 2H_2O$, CH_3OH–CH_2Cl_2.

‡ The compound numbering in the present zinc chlorins also indicates the carbon number in the covalent linker and "**D**" denotes that the C3^1–C3^2 covalent linkage is a double bond.

with $NaBH_4$ to give **6**. To convert **4D** to **6** more easily, we attempted direct introduction of a hydroxy group into the 3^2-position by anti-Markovnikov hydration of the 3-vinyl group. The reactive 13-keto group of **4D** was protected as its ethylene ketal according to the reported procedure to give **5D** in 90% yield (step i in Scheme 1).[13,14] Chlorin **5D** was carefully treated with BH_3–THF and successively treated with H_2O_2–NaOH (step ii). After the reaction mixture had been treated with dil. aq. HCl to eliminate the ketal-protection (step iii), a regioisomeric mixture of 3-(2-hydroxyethyl)chlorin **6** and 3-(1-hydroxyethyl)chlorin **7** (methyl bacteriopheophorbide *d*) was obtained in 51% yield from **5D**. The ratio of **6** : **7** was 33 : 1 by ^{1}H-NMR, indicating that the hydroboration regioselectively proceeded at the 3-vinyl group in anti-Markovnikov manner as expected. Chlorin **4D** (18%) was also obtained by ketal-deprotection of unchanged **5D** in the hydroboration (step ii). Slight reductive cleavage of either C13^1–O bond of the dioxolane ring in **5D** occurred during step ii to give 13^1-(2-hydroxyethoxy)chlorins (bottom drawing in Scheme 1).[15] Treatment of **5D** with excess of BH_3–THF gave a large amount of the undesired cleavage compounds. Regioisomers **6** and **7** were zinc-metallated and pure zinc chlorin **2** possessing a 2-hydroxyethyl group at the 3-position was isolated by high-performance liquid chromatography (HPLC). Overall yield from **4D** to **6** in the present synthetic procedures was 45% (= 0.9 × 0.51 × 33/34 × 100) and **4D** was recovered to the extent of 26% [= (0.1 + 0.9 × 0.18) × 100]. Therefore, yield of **4D** ⟶ **6** based on consumed **4D** is estimated to be 61% [= 0.45/(1 − 0.26) × 100], which is higher than that reported by Smith *et al.* (51% yield). Moreover, our method is advantageous over the previous procedures from the viewpoint of laboratory safety because highly toxic thallium compound and sulfur dioxide gas are not required.

Synthesis of zinc chlorins 3 and 3D

To synthesize 3-(3-hydroxypropyl)chlorin **3** (or **12**), we chose methyl pyropheophorbide-*d* (3-deethyl-3-formylphytochlorin methyl ester, **8**)[8,16] as a starting material (Scheme 2). We first examined a Wittig reaction of **8** with commercially available stable formylmethyl ylide **W-a** (Ph_3P=CHCHO, Chart 1). The

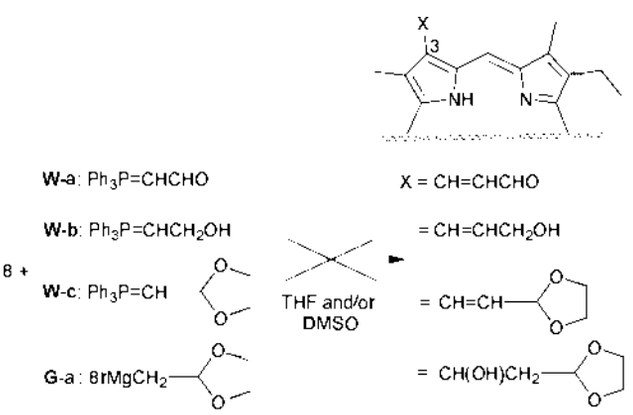

Chart 1

reaction in dichloromethane at room temperature did not progress and most of the starting material **8** was recovered. Increasing the reaction temperature (≈50 °C) did not promote the Wittig reaction and a further increase in temperature (≈70 °C) gave rise to degradation of **8**. Although other stable Wittig reagents such as Ph_3P=CHCOOCH$_3$ and Ph_3P=CHCN smoothly reacted with the 3-formyl group of **8** to provide the corresponding 3-(2-substituted ethenyl)chlorins,[16] highly stable Ph_3P=CHCHO (**W-a**) did not react because of the lower reactivity of the 3-formyl group of **8** than that in benzaldehyde.

We next examined Wittig reaction of **8** with unstable ylides,

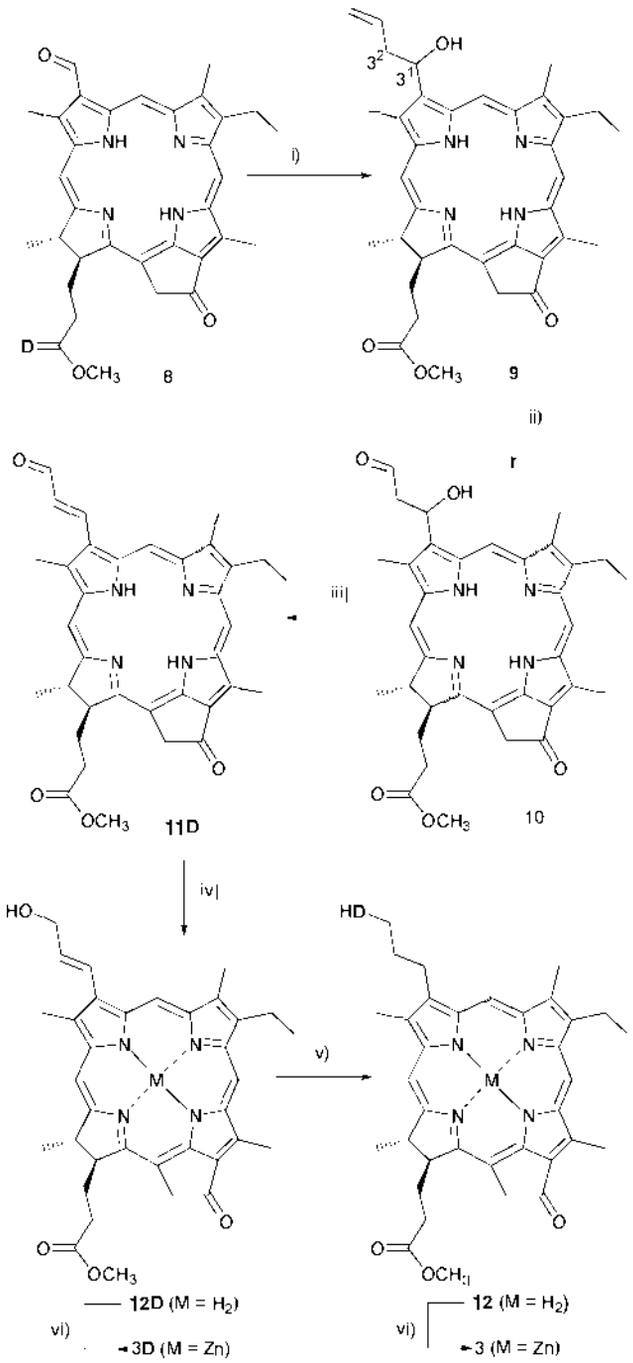

Scheme 2 *Reagents and conditions*: (i) CH_2=$CHCH_2Br$, In, aq. THF; (ii) OsO_4, $NaIO_4$ aq. AcOH–THF; (iii) PTSA, benzene, 50 °C; (iv) *t*-$BuNH_2$·BH_3, CH_2Cl_2; (v) H_2/PtO_2, THF; (vi) $Zn(OAc)_2$·$2H_2O$, CH_3OH–CH_2Cl_2.

2-hydroxyethylidenetriphenylphosphorane (**W-b**, Chart 1)[17] and 1,3-dioxolan-2-ylmethylenetriphenylphosphorane (**W-c**, Chart 1).[18] Ylides **W-b** and **W-c** were prepared from the corresponding phosphonium bromides by treatment with *n*-BuLi and lithium hexamethyldisilazane (LiHMDS) in THF, respectively, according to literature methods. When **8** was treated with the above two unstable ylides in dry THF, few desired coupling products were obtained, and **8** was predominantly recovered with a small amount of uncharacterizable degradation products. Unstable ylides **W-b** and **W-c** must have been decomposed before reacting with the less reactive 3-formyl group of **8**, which is consistent with our previous observation.[16] Treatment of **8** with *in situ* preparation of the above two ylides resulted in a drastic increase of the degradation products, indicating that **8** is sensitive to strong bases.

As an alternative method for the preparation of **3**, we examined Grignard reaction of **8** with commercially available 1,3-dioxolan-2-ylmethylmagnesium bromide (**G-a**, Chart 1). However, the reaction of **8** with **G-a** in dry THF provided no desired Grignard adduct, and undesired $C13^2$–$C17^3$ cyclized derivative of **8** was obtained in low yield together with recovered **8**.[19]

Our attempts at Wittig reaction of **8**§ described above led to the observation that the chlorin **8** is sensitive to strong bases and high reaction temperature (>70 °C) in addition to the low reactivity of the 3-formyl group in comparison with other formyl groups conjugated with a benzene-like aromatic ring. Mild conditions are necessary for the reaction of **8**. Indium-mediated Barbier-type reaction of allyl or propargyl halides with carbonyl compounds is one of the useful synthetic methods for functionalization of carbonyl groups under mild conditions. In the reaction, carbonyl compounds smoothly react with allyl or propargyl halides in an aqueous organic solution in the presence of indium at an ambient temperature to give Barbier/Grignard-type adducts in a considerably high yield.[20] We examined the indium-mediated Barbier type reaction of **8**. When an aq. THF solution of **8** and excess of allyl bromide (8 eq.) were stirred in the presence of indium powder (8 eq.) for 2 hours at room temperature, allylated chlorin **9** was obtained in a surprisingly high yield of over 80% (step i in Scheme 2). Prolonged reaction time (overnight) gave rise to additional allylation at the 13-keto group. Diastereomeric ratio of the 3^1-stereochemistry was almost 1 : 1 by ^{1}H-NMR. Subsequently, the vinyl group of **9** at the 3^2-position was oxidatively cleaved by OsO_4–$NaIO_4$ to give the corresponding aldehyde.[10] Although successful oxidation of **9** was ascertained by the typical CHO signal (δ 10 in $CDCl_3$) in the ^{1}H-NMR spectrum of the crude reaction mixture, isolation of **10** was difficult by flash column chromatography (FCC) due to its broadened elution with uncharacterizable side-products. Crude aldehyde **10** was easily dehydrated by mild heating (50 °C) in benzene containing a catalytic amount of toluene-*p*-sulfonic acid (PTSA) to afford pure chlorin **11D** in 59% isolated yield from **9** after simple FCC purification. As expected, dehydration of **10** smoothly progressed in comparison with that of the 3-(1-hydroxyethyl)chlorin **7** because of formation of a stable α,β-unsaturated aldehyde as the dehydration product. The resulting **11D** was a single stereoisomer with respect to the eth-3-enyl moiety and showed a coupling constant $^3J(3^1H–3^2H)$ = 16 Hz in its ^{1}H-NMR spectrum, indicating the *E*-configuration as drawn in Scheme 2. Chlorin **11D** shows a Q_y absorption maximum at 691 nm in CH_2Cl_2, which is red-shifted from that of unsubstituted vinylchlorin **4D** (667 nm) by the direct conjugation of the 3^2-formyl group with the chlorin chromophore through the eth-3-enyl moiety.[16] The red-shift is larger than those of the corresponding *E*-3^2-methoxycarbonyl (684 nm in CH_2Cl_2) and *E*-3^2-cyano derivatives (689 nm in CH_2Cl_2), which are obtained by Wittig reaction of **8** with Ph_3P=$CHCOOCH_3$ or Ph_3P=CHCN,[16] probably due to the stronger electron-withdrawing effect of the formyl group compared with that of methoxycarbonyl and cyano groups. Chlorin **11D** was easily converted into **12D** by reduction with *t*-$BuNH_2$·BH_3 in 92% yield. Hydrogenation of **12D** with H_2 over PtO_2 in THF gave the 3-(3-hydroxypropyl)chlorin **12** in moderate yield (81%). Finally, zinc-metallation of **12** gave the desired zinc chlorin **3**. In addition, zinc chlorin **3D** was prepared by zinc-metallation of **12D**.

To our knowledge, this is the first attempt of indium-mediated allylation of methyl pyropheophorbide-*d* **8**. The yield of allylation is very high. This reaction is useful for the introduction of various allyl-type substituents into a formyl group directly bound to a chlorin moiety. The indium-mediated Barbier-type reaction of **8** with various allyl and propargyl compounds will be reported elsewhere. Moreover, chlorin **11D** is a versatile precursor for preparation of intramolecular electron/energy-transfer systems because the reactive formyl group is directly linked to a rigid eth-3-enyl group that could spatially fix donor and acceptor chromophores.

§ Alternative synthetic approach *via* reduction of 3-[2-(methoxycarbonyl)ethenyl]chlorin by $LiA1H_4$ obtained by Wittig reaction of **8** with Ph_3=$CHCOOCH_3$ (ref. 18) gave desired chlorin **12** and **12D** (see supplementary data). However, overall yield from **8** to **12** was only 1.1%.

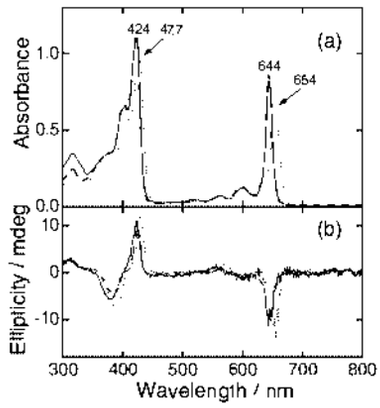

Fig. 3 Visible absorption (a) and CD spectra (b) of monomeric zinc chlorin **2** (solid curve), **3** (broken curve) and **3D** (dotted curve) in neat THF. Concentration of each solution is 15 μM.

Optical properties of monomeric zinc chlorins

Visible absorption spectra of monomeric **2** and **3** in neat THF are shown in Fig. 3a by solid and broken curves, respectively. Both **2** and **3** gave the same Soret and Q_y absorption maxima at 424 and 644 nm, respectively, which are almost identical to those of monomeric **1** in neat THF (424 and 646 nm). Both the full widths at half maxima (FWHMs[5]) of Q_y absorption bands of **2** and **3**, which result from molecular transition along with Q_y direction (N21---N23 axis in left drawing of Fig. 2), are 323 cm^{-1} and also identical to that of **1** (320 cm^{-1}). Extension of covalent linkage between the hydroxy group and the chlorin moiety does not electronically affect the absorption properties of monomeric zinc chlorins because there is no direct conjugation of the hydroxy group with the chlorin π-system and no strong inductive effect of the hydroxy group. Monomeric **3D** in THF has Soret and Q_y absorption maxima at 427 and 654 nm (dotted curve in Fig. 3a), which are almost identical to those of zinc complex of **4D** (427 and 655 nm). Red-shifts of these bands from those of monomeric **2** and **3** are attributed to direct conjugation of the $C3^1$–$C3^2$ double bond with the chlorin π-system.[21] The FWHM of Q_y absorption band of **3D** is broader (406 cm^{-1}) than those of **2** and **3** and also identical to that of zinc complex of **4D** (419 cm^{-1}). The fact that there is no absorption spectral difference between **3D** and the zinc complex of **4D** indicates that the 3^2-hydroxymethyl group does not electronically affect the absorption properties of eth-3-enylchlorins.

CD spectra of monomeric **2**, **3** and **3D** in neat THF gave small positive/negative and negative CD signals in the regions of the corresponding monomeric Soret and Q_y absorption bands, respectively (Fig. 3b); these are attributable to the small rotational strength of monomeric chromophores. Similarly to the visible absorption spectra, CD spectra of monomeric zinc chlorins **2**/**3** and **3D** were also identical to those of monomeric **1** and the zinc complex of **4D**, respectively.

Self-aggregation of zinc chlorin 2

Visible absorption spectra of zinc chlorins **2** and **1** in 1% THF–hexane under the same concentration (15 μM) are shown in Fig. 4. In 1% THF–hexane, zinc chlorin **2** gave new absorption bands in the longer-wavelength region in addition to the

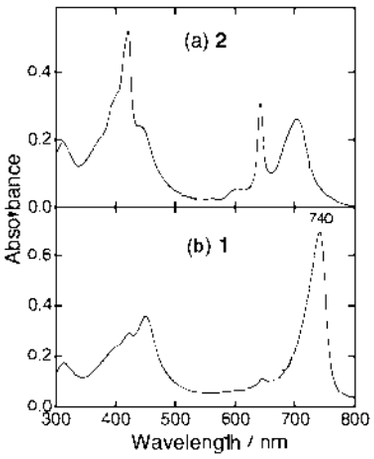

Fig. 4 Visible absorption spectra of **2** (a) and **1** (b) in 1% THF–hexane. Concentration of both the solutions is 15 μM.

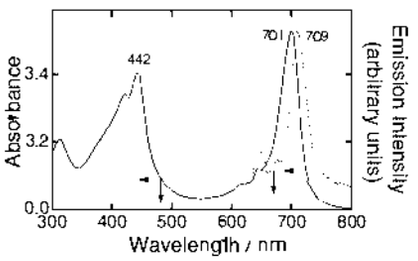

Fig. 5 Visible absorption (solid curve) and fluorescence spectra (excited at 440 nm, dotted curve) of **2** (15 μM) in 0.1% THF–hexane.

residual monomeric bands at 421 and 643 nm (Fig. 4a). The new absorption bands growing in the nonpolar organic solvents indicate that **2** self-aggregated to form oligomers in which composition molecules electronically interacted to absorb longer-wavelength light in comparison with the monomer in neat THF. Comparison with the intensity of the residual monomeric band at around 643 nm in 1% THF–hexane demonstrates that roughly 20% (calculated from the intensity of residual monomeric absorption) of **2** remained as the monomer despite only a slight proportion (< 5%) of monomeric **1** being present in 1% THF–hexane (Figs. 4a and 4b). The monomer $\rightleftharpoons$ aggregate equilibrium of **2** in solution lies toward a more monomeric state than that of **1**, indicating a lower aggregation ability for **2** than for **1**.

Visible absorption and fluorescence emission spectra of **2** in 0.1% THF–hexane are shown by solid and dotted curves in Fig. 5, respectively. Decrease of THF content in hexane (1 $\longrightarrow$ 0.1%) enhanced the absorption bands of the aggregates of **2** (15 μM in monomer base) in compensation for monomeric bands (solid curve in Fig. 5). In comparison with the monomer in THF, the absorption bands of the aggregates were broadened (FWHM of Q_y band is 765 cm^{-1}), moved to 442 (Soret) and 701 nm (Q_y), and red-shifted by 960 (Soret) and 1260 cm^{-1} (Q_y). These spectral changes are characteristic of the self-aggregates of chlorosomal chlorophylls. However, the red-shifted values of the absorption bands of the aggregates of **2** from the monomeric bands are smaller than those of **1** [1360 (Soret) and 1940 cm^{-1} (Q_y)] in 1% THF–hexane (Fig. 4b), indicating weaker excitonic interaction in the aggregates of **2** and smaller aggregation number. The fluorescence spectrum of **2** in 0.1% THF–hexane showed the emission at 709 nm attributed to the 701-nm-absorbing aggregates of **2** (dotted curve in Fig. 5). The emission is also less red-shifted from the monomeric Q_y emission (644 nm in THF) than those of the aggregates of **1** (646 nm in THF $\longrightarrow$ 745 nm in 1% THF–hexane).

In 1% THF–hexane, **2** exhibited specific CD signals in the red-shifted Q_y band region (data not shown). In 0.1% THF–

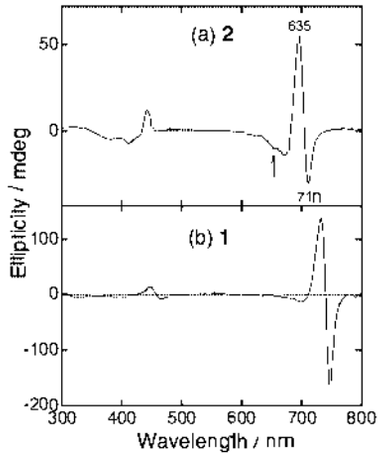

Fig. 6 CD spectra of **2** in 0.1% THF–hexane (a) and **1** in 1% THF–hexane (b). Concentration of both the solutions is 15 μM.

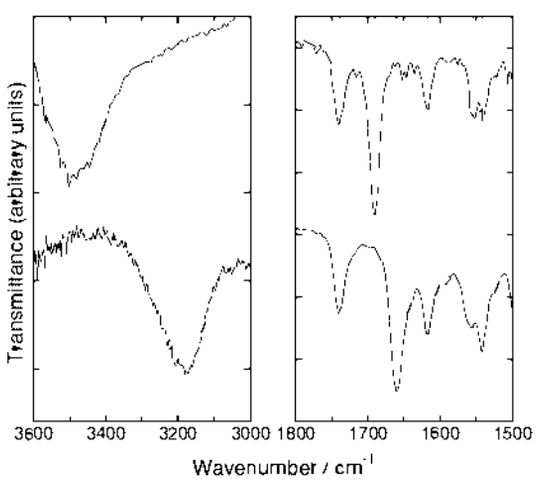

Fig. 7 IR spectra of monomeric **2** in THF (upper) and the solid thin film of **2** (lower) in the hydroxy (left), and carbonyl and chlorin skeletal C–C/C–N vibrational regions (right).

hexane containing a larger amount of aggregates, such CD signals were enhanced and the signal shape remained nearly unchanged (Fig. 6a). This demonstrates that the observed CD signals were derived from the 701-nm-absorbing aggregates of **2**: the negative small peak at around 650 nm (arrow in Fig. 6a) is ascribable to residual monomeric **2**. The CD signals are composed of a sharp and intense reverse S-shaped signal in the longer wavelength region and a relatively broad and small S-shaped signal in the shorter-wavelength region. Such a signal pattern resembles that of the aggregates of **1** (Fig. 6b). The observation is ascribed to the strong exciton coupling among Q_y transition moments of composition molecules, which are close and parallel to each other and aligned to the long axis of aggregates in a highly ordered supramolecular structure.[8,19] Both the observed spectra for the aggregates of **2** and **1** could be simulated by the sum of two sign-reversed exciton-type components. These CD components would originate from the non-degenerate excitonic transitions of a major oligomeric species.[22] Thus, this CD study strongly suggests that the orientation of the pigments in the aggregates of **2** is not greatly different from that of the aggregates of **1**.

Fig. 7 shows the IR spectra of monomeric **2** in THF and the solid film of **2** in the C=O, chlorin skeletal C–C and C–N (right) and O–H (left) vibrational regions. Zinc chlorin **2** in the solid film showed three bands in the range of 1500–1630 cm^{-1}, of which peak positions are identical to those of monomeric **2** in THF (Fig. 7). These three bands at 1540, 1553 and 1617 cm^{-1}, arising from the C–C and C–N vibrations of the chlorin

skeleton, show the presence of a 5-coordinated central Zn atom in comparison with previous assignments for the solid film aggregates of **1**.[8,23] Therefore, **2** in the solid film as well as in THF possesses a central zinc with a single axial O-ligand (O ··· ZnN_4). The band peaking at 1660 cm^{-1} in the solid film of **2** is attributed to the 13-C=O stretching mode, which is drastically downshifted (30 cm^{-1}) from that in monomer solution at 1690 cm^{-1}, free from any interaction. The large downshifted value indicates the formation of the C=O ··· H–O ··· Zn linkage in the film of **2**.[8] The bands peaking at 1738 cm^{-1} in both IR spectra are attributed to a carbonyl stretching mode of the 17^2-$COOCH_3$ group. The lack of shift of these bands demonstrates that the 17^2-$COOCH_3$ is free from any interaction in the film and monomeric state. The O–H stretching band in the solid film of **2** peaked at 3200 cm^{-1}, which is greatly downshifted by 300 cm^{-1} from the O–H stretching band in monomer solution at 3500 cm^{-1}, normally hydrogen-bonding with a THF molecule. The large downshift is ascribable to strong hydrogen bonding of the 3^2-OH group in the film. The hydrogen bond is enhanced by the coordination of the hydroxy oxygen to the central zinc. From the visible absorption and CD spectral similarity between the solid film and the solution aggregates, it is plausible that IR spectra of the solid film reflect the structural characteristics of solution aggregates. Thus, the IR study revealed that **2** in aggregates formed the C=O ··· H–O ··· Zn linkage as well as **1** did.

One of the reasons for the lower aggregation ability of **2** than of **1** is an enhancement of conformational freedom of the interactive hydroxy group in a molecule, allowed by the more flexible ethylene linker of **2** than the methylene linker of **1**. This is in good agreement with our previous study; conformationally flexible interactive sites in a molecule suppress the aggregation ability of metallochlorins because they can take various molecular conformations.[21] Another reason may lie in the ethylene linker of **2** being bulkier than the methylene linker of **1**. The bulkier linker is disadvantageous for molecular packing in the self-aggregates, suppressing the formation of tight self-aggregates. CD and IR studies showed that **2** can form aggregates that possess the same molecular orientation (ordered orientation) and the same interaction motif among the three interactive sites (the intermolecular C=O ··· H–O ··· Zn linkage) as the aggregates of **1**, while **2** aggregated with a weaker excitonic interaction state and in smaller aggregation number than **1** did, from the visible spectral analyses. The longer ethylene linker must expand the face-to-face distance between the neighboring molecules linked by an HO ··· Zn bond in the aggregates of **2**. Obviously, this situation weakens the π–π interaction between the chlorin π-planes, decreasing the excitonic interaction and the size of aggregates. Both the weaker excitonic interaction and the smaller aggregation number diminish the red-shift of electronic absorption of the aggregates of **2**.

Self-aggregation of zinc chlorin 3

The visible absorption spectrum of zinc chlorins **3** (15 μM) in 1% THF–hexane gave no new red-shifted absorption bands (data not shown), and was almost identical to that of the monomer in THF except for slight blue-shifts probably due to a decrease in the solvent polarity. In 1% THF–hexane, almost all **3** remained as the monomer, while 20% of **2** and a slight proportion (<5%) of **1** remained as the monomer in 1% THF–hexane (Figs. 4a and 4b). Therefore, the monomer ⇌ aggregate equilibrium of **3** in solution lies in the greatest extent of monomeric state among the three zinc chlorins, indicating the lowest aggregation ability of **3**. With a decrease of the THF concentration in the hexane solution, **3** (15 μM) began to associate and gave broadened absorption bands in 0.5% THF–hexane (solid curve in Fig. 8a). After preparation of the solution, these new bands gradually grew concomitantly with the decrease of the monomeric absorption bands (dotted curves in Fig. 8a), and the spectral change finished 10 minutes later (broken curve in Fig. 8a). During the spectral change, the Q_y maxima of the red-shifted bands remained in the range 702–704 nm, indicating an increase of the same aggregated species. Such a time-dependent aggregation was not observed in the aggregation of **1** and **2** in THF–hexane admixture in any ratio. Therefore, formation of the aggregates in **3** is slower than in **1** and **2**.

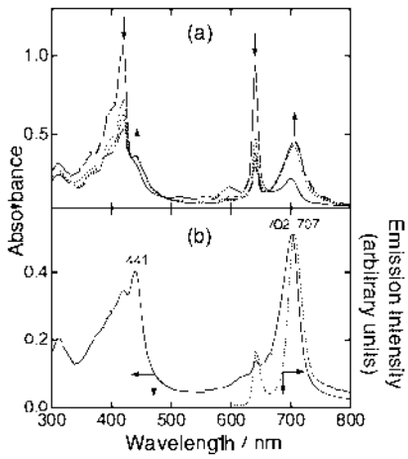

Fig. 8 Visible absorption and fluorescence spectra of **3**. (a) Time-dependent visible absorption spectral change of **3** (15 μM) in 0.5% THF–hexane; solid curve, immediately after preparation of the solution; dotted curves, 3–9 min later; broken curve, steady state 10 min later. (b) Visible absorption (solid curve) and fluorescence spectra (excited at 440 nm, dotted curve) of **3** (15 μM) in 0.1% THF–hexane.

Visible absorption and fluorescence emission spectra of **3** in 0.1% THF–hexane are shown by solid and dotted curves in Fig. 8b, respectively. In 0.1% THF–hexane, **3** (15 μM) gave dominant absorption bands of the aggregates having absorption maxima at 440 (Soret) and 702 nm (Q_y), immediately after preparation of the solution (solid curves Fig. 8b). The Q_y absorption maximum is almost identical to that in 0.5% THF–hexane. In comparison with the monomer in THF, the absorption bands of the aggregates were more broadened (FWHM of Q_y band is 730 cm^{-1}) and red-shifted by 909 (Soret) and 1280 cm^{-1} (Q_y), respectively. The red-shifted values of the absorption bands of the aggregates of **3** from the monomeric bands are considerably smaller than those of **1** [1360 (Soret) and 1940 cm^{-1} (Q_y)] in 1% THF–hexane (Fig. 4b). This is attributed to a weaker excitonic interaction and a smaller aggregation number. However, these red-shifted values of **3** are nearly identical to those of **2** [960 (Soret) and 1260 cm^{-1} (Q_y)], indicating the same degree of excitonic interaction and aggregation number in each aggregate. The aggregates of **3** emitted at 707 nm (dotted curve in Fig. 8b), for which the red-shifted value from the monomeric emission (644 nm in THF) is smaller than that of the aggregates of **1** (646 nm in THF ⟶ 745 nm in 1% THF–hexane) but almost the same as that of the aggregates of **2** (644 nm in THF ⟶ 709 nm in 0.1% THF–hexane).

The 0.5% THF–hexane solution of **3** (15 μM) immediately after preparation gave small CD signals in the red-shifted Soret and Q_y band-regions (solid curve in Fig. 9a). The CD peaks gradually increased in intensity while retaining the signal shape (dotted curves in Fig. 9a) to give finally the CD spectrum shown by the broken curve in Fig. 9a (10 min after preparation). This result corresponds to the slow aggregation process of **3** shown by time-dependent visible spectral changes in the same solution (Fig. 8a). The 0.1% THF–hexane solution of **3** gave CD signals whose shape was almost identical to those observed in 0.5% THF–hexane (solid curve Fig. 9b). This indicates that the aggregate species formed in 0.5% and 0.1% THF–hexane are identical. The CD signal in Q_y region is composed of a single reverse S-shaped signal. The signal shape is quite asymmetric,

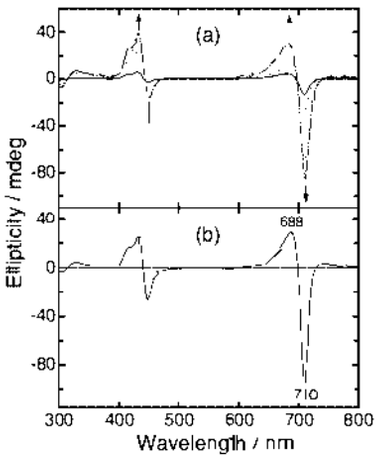

Fig. 9 CD spectra of **3**. (a) Time dependent CD spectral change of **3** (15 μM) in 0.5% THF–hexane; solid curve, immediately after preparation of the solution; dotted curves, at 3–9 min later; broken curve, steady state at 10 min later. (b) CD spectrum of **3** (15 μM) in 0.1% THF–hexane.

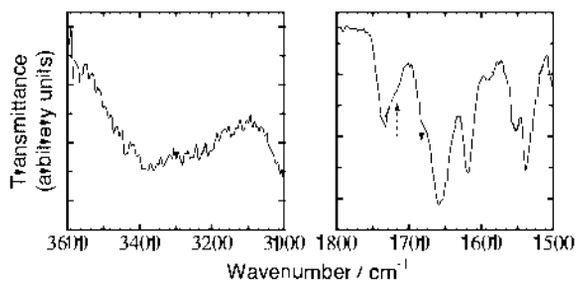

Fig. 10 IR spectra of solid thin film of aggregated **3** in the hydroxy (left), and carbonyl and chlorin skeletal C–C/C–N vibrational band regions (right).

where the negative signal peaking at 710 nm is approximately three-fold larger than the positive signal peaking at 688 nm. Such a CD signal in the Q_y region is clearly distinguishable from those of **1** and **2** (Fig. 6). Furthermore, it is worth pointing out that the aggregates of **3** gave intense reverse S-shaped CD signal in the Soret region in comparison with those of **1** and **2**; the ellipticities of CD peaks in aggregated solutions are 14/−8 in **1** (Fig. 6b), −4/12 in **2** (Fig. 6a) and 27/−33 mdeg in **3** (Fig. 9b). Thus, CD spectra of the aggregates of **3** are remarkably different from those of **1** and **2**. This demonstrates that the type of excitonic coupling among the pigments in the aggregates of **3** is different from those in the aggregates of **1** and **2**, indicating that orientation of the pigments in the aggregates of **3** is also different; the aggregates of **3** may be less ordered in the supramolecular structure than are those of **1** and **2**. The difference between the CD spectra of the aggregates of **2** and **3** whose visible spectra are almost identical to each other does not conflict with the higher sensitivity of CD spectra for small structural changes of chlorosomal Chl supramolecules in comparison with absorption spectra.[24,25]

Fig. 10 shows IR spectra of the solid thin film of aggregated **3** whose supramolecular structure had been confirmed to be identical to that in 0.1% THF–hexane by visible absorption and CD spectral similarity between the two aggregated states (data not shown). The solid film of **3** showed three bands at 1540, 1553 and 1617 cm^{-1}, arising from the C–C and C–N vibrations of the chlorin skeleton. These peak positions are identical to those of monomeric **3** in THF and solid aggregates of **1** and **2**, indicating the presence of a 5-coordinated central Zn atom. Therefore, the central zinc in the solid film of **3** was also axially ligated by a single O-ligand (O ··· ZnN_4). Although the 13-C=O stretching band in the solid film of **3** dominantly emerged at 1660 cm^{-1}, which is identical to that observed in the solid film of **2**, a clear shoulder was exhibited in the higher frequency region of the major 13-C=O band (solid arrow in Fig. 10). The observation indicates that a small proportion of the 13-C=O groups in the solid aggregates of **3** is in a different situation from the C=O ··· H–O ··· Zn where a large proportion of the 13-C=O group is involved. Such a chemical environment is ascribable to a relatively weak C=O ··· H–O(··· Zn) bond as well as normal hydrogen bond (C=O ··· H–O) and direct coordination to central zinc (C=O ··· Zn). The carbonyl stretching band of the 17^2-$COOCH_3$ group in the solid film of **3** emerged at 1738 cm^{-1}, unshifted from the monomeric band in THF. However, a clear shoulder was observed in the lower-frequency region of the band (broken arrow in Fig. 10). This indicates that a small proportion of 17^2-$COOCH_3$ in the solid film of **3** formed a certain kind of interaction such as 17^2-C=O ··· H–O(··· Zn) and/or 17^2-C=O ··· Zn, while most of 17^2-C=O was free from any interaction, as in the case of **2**. The O–H stretching band of **3** in the solid aggregates was broadened in the range 3100–3500 cm^{-1}. This clearly contrasts with the relatively sharp and largely downshifted O–H stretching band of **2** (3200 cm^{-1}) in the solid film. The broadening is very likely attributable to the overlap of several O–H stretching bands originating from heterogeneously interacting O–H groups in strength and variety. This is consistent with the presence of the less downshifted 13-C=O stretching band and the slightly downshifted carbonyl stretching band of the 17^2-$COOCH_3$ group. Thus, the IR study demonstrated that the aggregates of **3** contain not only the major strong C=O ··· H–O ··· Zn linkage but also other minor interaction motifs such as relatively weak C=O ··· H–O ··· Zn linkage, C=O ··· Zn, 17^2-C=O ··· H–O(··· Zn) and 17^2-C=O ··· Zn as intermolecular noncovalent linkages.

The low aggregation ability of **3** is ascribable to much enhancement of conformational freedom of the interactive hydroxy group in a molecule and the bulkiness of the linker trimethylene moiety in **3**. Reflecting the long linker, the face-to-face distance between the composition molecules in the aggregates of **3** was expanded more than that in the aggregates of **1**, as shown by the red-shifted values of the aggregates. Nevertheless with the longer trimethylene linker of **3** than the ethylene linker of **2**, both the aggregates of **3** and **2** showed almost identical red-shifted values, indicating that the face-to-face distance between the neighboring molecules linked by an HO ··· Zn bond in the aggregates of **3** is comparable to those in the aggregates of **2**. This finding demonstrates that the trimethylene moiety of **3** and the ethylene moiety of **2** in the aggregates maintain the same distance between the 3-position and the ω-hydroxy group. Obviously, conformational strain of the trimethylene moiety in aggregated **3** is larger than that of the ethylene moiety in aggregated **2**. Therefore, conformational restriction of the linker moiety through coordination of a ω-hydroxy group to the central zinc of a neighboring molecule by aggregation of **3** is larger than that by aggregation of **2**. This leads to substantial dissociation of the HO ··· Zn bond in the aggregation of **3**, which may further suppress the aggregation of **3** and also may make the aggregation of **3** slower than that of **1** and **2** as shown by the time-dependent visible and CD spectral change in 0.5% THF–hexane. Moreover, the ω-hydroxy group of **3**, attached to the conformationally strained trimethylene linker in the aggregated state, must more or less diverge from the Q_y molecular axis. This situation may disturb the orientation of composition molecules and prevent the formation of the homogeneously strong intermolecular C=O ··· H–O ··· Zn linkage as shown by CD and IR spectral analyses.

Self-aggregation of zinc chlorin 3D

In 1% THF–hexane, **3D** (15 μM) gave a Q_y absorption maximum at 680 nm in addition to a residual monomeric band at 652 nm, where the two bands overlapped each other con-

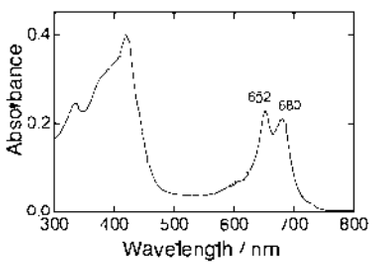

Fig. 11 Visible absorption spectrum of **3D** (15 μM) in 1% THF–hexane.

siderably (Fig. 11). Spectral deconvolution revealed that the spectrum in the Q_y region was the sum of a single Gaussian component peaking at 680 nm and the monomeric Q_y absorption band peaking at 652 nm observed in 5% THF–hexane (data not shown). The FWHM of the 680 nm absorption band was 650 cm^{-1}, 1.6-fold broader than that of the monomer (400 cm^{-1}). The band broadening is characteristic of self-aggregation, showing the 680-nm-absorbing species to be the self-aggregates of **3D**. The 680 nm absorption band is red-shifted by 580 cm^{-1} from the monomeric Q_y band in THF (654 nm). The significantly smaller red-shift of the Q_y absorption band of the aggregates of **3D** than those of **1** (1940 cm^{-1}, Fig. 4b), **2** (1260 cm^{-1}, Fig. 4a) and **3** (1280 cm^{-1}, Fig. 8b) indicates the considerably smaller aggregation number and/or weaker excitonic interaction of the aggregates of **3D**. The absorption intensities of the 680-nm-absorbing aggregates and the residual monomer are 0.14 and 0.12, respectively, and the quotient of absorption intensity of the aggregates over the consumed monomer is 0.27. This value is much smaller than those of the aggregation of **1** (0.7), **2** (0.68) and **3** (0.63). This is probably due to inhomogeneity of the solution by the formation of microscopic precipitates, because the aggregated solution of **3D** gave macroscopic precipitates from the preparation after storage for only a few minutes. This prevented us from performing any spectral analyses other than rapid measurements of the visible spectrum in solution. In 0.1% THF–hexane, **3D** immediately formed precipitates just after preparation. Such a precipitation could not be observed in 0.1% THF–hexane solution of **2** and **3**, even after storage for several hours. **3D** possesses the planar 3-CH=CH-linker, which is more favorable for the molecular packing in the supramolecule than are **2** and **3** involving a fully saturated alkyl linker.

During formation of the macroscopic precipitates in the 1% THF–hexane solution of **3D**, no red-shift was observed in the 680 nm absorption band. Moreover, supernatant hexane solution after several minutes was completely depleted of the 680-nm-absorbing aggregates. Shaking the precipitated solution disrupted the macroscopic precipitates and the absorption spectrum again showed a 680 nm absorption band. These findings indicate that the 680 nm-absorbing aggregates were soluble, large aggregates and a building block of macroscopic precipitates.

The IR spectrum of the precipitates of **3D** was measured (see supplementary data †). The O–H, 17^2-C=O, 13-C=O and the three chlorin-skeletal C–C and C–N vibrational bands emerged at 3180, 1738, 1653, 1614, 1552 and 1539 cm^{-1}, respectively. These band positions are characteristic of the formation of the C=O ··· H–O ··· Zn linkage as explained in the IR study of **2** (Fig. 7). Moreover, no shoulder or band broadening in the 13-C=O, 17^2-C=O and O–H stretching bands was observed, while they *were* observed in the IR spectrum of aggregated **3** (Fig. 10). These results demonstrate that **3D** forms a homogeneous, strong C=O ··· H–O ··· Zn linkage in the precipitates. Therefore, the precipitates and their building blocks, the 680-nm-absorbing aggregates of **3D**, are structurally ordered, large aggregates, similar to the aggregate structure of **1** reported in our previous study.[8]

The smaller red-shift of the Q_y absorption band in the aggregates of **3D** than those of the aggregates of **2** and **3** as well as **1** despite their large size would be due to the significantly weaker excitonic interaction between the composition molecules in the aggregates. As expected, the planar and rigid 3-CH=CH- linker does not separate the two neighboring molecules linked by an HO ··· Zn bond toward the vertical direction with respect to the chlorin π-plane but does separate them toward the horizontal direction compared with those of **1**. This situation decreases the overlapping region between the chlorin π-systems in the aggregates of **3D**, weakening the excitonic interaction in the supramolecule.

The importance of a methylene linker between the interactive hydroxy group and the chlorin moiety for the formation of antenna aggregates

The flexible, long linker expanded the face-to-face distance between the composition molecules in the aggregates of **2** and **3** compared with those in the aggregates of **1**. Moreover, composition molecules in the aggregates of **3** were prevented from associating regularly and from forming a homogeneously strong intermolecular C=O ··· H–O ··· Zn linkage. The rigid, long linker of **3D** decreases the overlapping region between the chlorin π-planes in the aggregated state. These aggregations of **2**, **3** and **3D** described here are disadvantageous for the light-harvesting antenna pigments in chlorosomes for the following three reasons. (i) **2**, **3** and **3D** self-aggregated to form relatively unstable oligomers. (ii) Unfavorable intermolecular interactions in the self-aggregates may result in structural defects in the aggregates like a lattice defect in crystals. Such defects are disadvantageous for efficient energy migration in the aggregates. (iii) The excitonic interaction among pigments in the aggregates of **2**, **3** and **3D** was weakened and thereby these Q_y fluorescence bands appeared in a shorter-wavelength region. This is energetically disadvantageous for efficient energy transfer to BChl-*a* in a baseplate.[26] It is concluded that the methylene linkage between the interactive hydroxy group and the chlorin moiety in the naturally occurring chlorosomal Chls as well as the model pigments such as **1** is necessary for the formation of the antenna aggregates appropriate for the efficient light-harvesting, energy-migration and energy-transfer.

Experimental

Instrumentation

Visible absorption and CD spectra were measured in air-saturated solvents at room temperature on a Hitachi U-3500 spectrophotometer and a JASCO J-720W spectropolarimeter, respectively. ^{1}H-NMR measurements were performed on a Bruker AC-300 MHz NMR spectrometer. Fast-atomic bombardment (FAB)–mass spectra (MS) were recorded on a JEOL HX-100 spectrophotometer; FAB-MS samples were dissolved in dichloromethane, and *m*-nitrobenzyl alcohol was used as the matrix. HPLC was carried out with a Shimadzu LC-10AS pump, and an SPD-M10AV visible detector. Fourier transform (FT)-IR spectra were recorded at room temperature on a Shimadzu FTIR-8600 spectrophotometer; a solution was measured in a KBr cell and an aggregate film on a thin-aluminium-film-coated glass by means of reflection absorption spectroscopy through a Shimadzu AIM-8000R microscope.

Materials

THF and hexane for visible, CD and IR spectra were freshly distilled over CaH_2 before use. BH_3 (THF solution, 1.00 M) and 1,3-dioxolan-2-ylmethylmagnesium bromide (**G-a**, hexane solution, 0.95 M) were purchased from Aldrich. Formylmethylenetriphenylphosphorane (**W-a**) and (2-hydroxyethyl-(triphenyl)phosphonium bromide for the preparation of ylide

W-b were purchased from Wako Pure Chemical Industries. 1,3-Dioxolan-2-ylmethyl(triphenyl)phosphonium bromide for the preparation of ylide **W-c** was purchased from Tokyo Chemical Industry. FCC was carried out on silica gel (Merck Kiesel gel 60, 9358). HPLC was performed with packed ODS columns (Cosmosil 5C18AR, Nacalai Tesque, 6.0 × 250 mm). All synthetic zinc chlorins and their intermediates were characterized by their visible, ^{1}H-NMR and FAB-MS spectra. Ketal-protection and -deprotection of 13-keto group were done according to the procedures reported by Tamiaki *et al.*[14] which are slight modifications of the original by Pandey *et al.*[13] Oxidative cleavage of the vinyl group,[21] reduction of the formyl group[21] and zinc-metallation[27] were done according to reported procedures. Methyl pyropheophorbide-*a*[8] **4D**, ketal-protected methyl pyropheophorbide-*a* **5D**,[13,14] and methyl pyropheophorbide-*d*[8] **8** were prepared from modification of Chl-*a* according to reported procedures. All synthetic procedures were done in the dark.

Synthesis of zinc methyl 3-devinyl-3-(2-hydroxyethyl)pyropheophorbide-*a* [3^2-hydroxyphytochlorinatozinc(II) methyl ester 2]

To a dry THF (15 ml) solution of the chlorin **5D** (40 mg) was added dropwise BH_3–THF (0.03 M; 30 ml) under argon atmosphere at room temperature with vigorous stirring. After stirring of the mixture for 3 h, ethanol (2 ml) and aq. NaOH (3.0 M; 2 ml) were added at −10 °C and then ice-chilled 30% aq. H_2O_2 (2 ml) was added at 0 °C. After stirring for 1.5 h, the solution was poured into brine and extracted with several portions of $CHCl_3$ and the combined organic phases were washed with brine and dried over Na_2SO_4. After evaporation of the solvents, the residue was dissolved in acetone (27 ml) and then conc. HCl (0.2 ml) was added with stirring. The reaction mixture was stirred for 10 min, poured into water, and extracted by CH_2Cl_2, and the extract was washed successively with 4% aq. $NaHCO_3$ and water, and dried over Na_2SO_4. The solvents were evaporated off and the residue was purified by FCC to give **4D** (6.7 mg, 18% yield, 5% EtO_2–CH_2Cl_2) and a 33 : 1 mixture of 3-(2-hydroxyethyl)chlorin **6** and 3-(1-hydroxyethyl)chlorin **7** (19.5 mg, 51% yield, 1% CH_3OH–CH_2Cl_2); λ_{max}/nm (CH_2Cl_2) = 658 (relative intensity, 39%), 602 (7.0), 536 (7.8), 503 (9.9), 408 (100), 396 sh (80); ^{1}H-NMR ($CDCl_3$) δ (major **6**) 9.48, 9.26, 8.50 (each 1H, s, 5-, 10-, 20-H), 5.23, 5.07 (each 1H, d, J = 20 Hz, 13^1-CH_2), 4.46 (1H, q, J = 7 Hz, 18-H), 4.37 (2H, t, J = 7 Hz, 3^1-CH_2), 4.27 (1H, d, J = 8 Hz, 17-H), 4.12 (2H, t, J = 7 Hz, 3-CH_2), 3.70 (2H, q, J = 8 Hz, 8-CH_2), 3.64, 3.60, 3.26, 3.25 (each 3H, s, 2-, 7-, 12-CH_3, $COOCH_3$), 2.45–2.73, 2.14–2.36 (each 2H, m, 17-CH_2CH_2), 1.80 (3H, d, J = 7 Hz, 18-CH_3), 1.69 (3H, t, J = 8 Hz, 8^1-CH_3), 0.45, −1.68 (each 1H, s, NH); MS (FAB) (Found: M$^+$ 566, Calc. for $C_{34}H_{38}N_4O_4$: *M*, 566).

The above mixture of metal-free chlorins **6** and **7** was zinc-metallated[27] and purified by HPLC (Cosmosil, CH_3OH–water 8 : 1; 1.0 ml min^{-1}) to give the title compound **2** (t_R 6.6 min) and the zinc complex of **7** (t_R7.7 min). The separation ratio was 1.6. **2**: λ_{max}/nm (THF) 644 (rel. 73%), 599 (10), 564 (5.5), 520 (3.6), 424 (100), 403 (57); ^{1}H-NMR (10% v/v CD_3OD–$CDCl_3$) δ 9.35, 8.95, 8.16 (each 1H, s, 5-, 10-, 20-H), 5.10, 4.92 (each 1H, d, J = 20 Hz, 13^1-CH_2), 4.29 (1H, q, J = 7 Hz, 18-H), 4.12 (2H, t, 3^1-CH_2), 4.05–4.20 (3H, m, 3-CH_2 + 17-H), 3.61 (2H, q, J = 8 Hz, 8-CH_2), 3.50, 3.41, 3.12, 3.10 (each 3H, s, 2-, 7-, 12-CH_3, $COOCH_3$), 2.36–2.60, 2.07–2.34 (each 2H, m, 17-CH_2CH_2), 1.66 (3H, d, J = 7 Hz, 18-CH_3), 1.58 (3H, t, J = 8 Hz, 8^1-CH_3); MS (FAB) (Found: M$^+$, 628. Calc. for $C_{34}H_{36}N_4O_4{}^{64}Zn$: *M*, 628).

Synthesis of zinc 3-devinyl-3-(3-hydroxypropyl)pyropheophorbide-*a* [3^2-(hydroxymethyl)phytochlorinatozinc(II) methyl ester 3]

To a stirred aq. THF solution (15 ml; THF–water 2 : 1) of methyl pyropheophorbide-*d* **8**, (65 mg) were added allyl bromide (300 mg) and indium powder (90 mg). After stirring of the mixture for 1.5 h at room temperature under nitrogen atmosphere, indium powder was filtered off and washed with CH_2Cl_2. The organic layer was washed with water three times, and dried over Na_2SO_4. The solvents were evaporated off and the residue was purified by FCC (1% CH_3OH–CH_2Cl_2) and then recrystallized from CH_2Cl_2–hexane to give 3-(1-hydroxybut-3-enyl)chlorin **9** (57 mg) in 82% yield. The 3^1-stereoconfiguration is a 1 : 1 mixture of *R* and *S*. For compound **9**: λ_{max}/nm (CH_2Cl_2) 661 (rel. 45%), 605 (7.4), 537 (8.7), 504 (9.5), 410 (100), 398 sh (87); ^{1}H-NMR ($CDCl_3$) δ 9.54/9.58, 9.24/9.25, 8.44/8.46 (each 1H, s, 5-, 10-, 20-H), 6.09/6.12 (1H, t, J = 8 Hz, 3-CH), 5.90–6.05 (1H, m, 3^2-CH), 5.25 (1H, d, J = 17 Hz, *E*-3^3-CH), 5.15 (1H, d, J = 10 Hz, *Z*-3^3-CH), 5.07/5.13, 4.95/4.99 (each 1H, d, J = 20 Hz, 13^1-CH_2), 4.38 (1H, q, J = 8 Hz, 18-H), 4.08–4.20 (1H, m, 17-H), 3.64/3.65, 3.51, 3.34/3.35, 3.19/3.20 (each 3H, s, 2-, 7-, 12-CH_3, $COOCH_3$), 3.60 (2H, q, J = 8 Hz, 8-CH_2), 3.05–3.20 (2H, m, 3^1-CH_2), 2.88/2.96 (1H, s, OH), 2.45–2.67, 2.03–2.37 (each 2H, m, 17-CH_2CH_2), 1.72/1.74 (3H, d, J = 8 Hz, 18-CH_3), 1.64 (3H, t, J = 8 Hz, 8^1-CH_3), −0.01/0.06, −2.04/−1.98 (each 1H, s, NH); MS (FAB) (Found: M$^+$, 592. Calc. for $C_{36}H_{40}N_4O_4$: *M*, 592).

The above vinylchlorin **9** (60 mg) was oxidized[21] by OsO_4 (*ca.* 5 mg), $NaIO_4$ (140 mg) and AcOH (180 µl) in water (1.1 ml)–THF (10 ml) and roughly purified by FCC (0.5–2.5% CH_3OH–CH_2Cl_2) to give a crude diastereomeric mixture of the 3-(1-hydroxy-2-formylethyl)chlorin **10** [^{1}H-NMR ($CDCl_3$) δ = 10.03 (1H, s, CHO)].

To a benzene solution (25 ml) of the entire crude sample was added PTSA (20 mg) with stirring. After stirring for 30 min at 50 °C under nitrogen atmosphere, the solution was poured into ice–water, the aqueous layer was extracted with several portions of CH_2Cl_2 and combined organic fractions were washed successively with 4% aq. $NaHCO_3$ and water, then dried over Na_2SO_4. The solvents were evaporated off and the residue was purified by FCC (5–10% Et_2O–CH_2Cl_2) and recrystallized from CH_2Cl_2–hexane to give the 3-(2-formylvinyl)chlorin **11D** (34 mg) in 59% yield from **9** in the above two steps: λ_{max}/nm (CH_2Cl_2) 691 (rel. 65%), 629 (8.9), 552 (13), 520 (14), 420 (100); ^{1}H-NMR ($CDCl_3$) δ 10.14 (1H, d, J = 7 Hz, CHO), 9.59, 9.46, 8.75 (each 1H, s, 5-, 10-, 20-H), 8.89 (1H, d, J = 16 Hz, 3-CH), 7.36 (1H, dd, J = 7, 16 Hz, 3^1-CH), 5.32, 5.17 (each 1H, d, J = 20 Hz, 13^1-CH_2), 4.55 (1H, dq, J = 2, 7 Hz, 18-H), 4.36 (1H, d, J = 8 Hz, 17-H), 3.72 (2H, q, J = 8 Hz, 8-CH_2), 3.70, 3.62, 3.54, 3.28 (each 3H, s, 2-, 7-, 12-CH_3, $COOCH_3$), 2.50–2.80, 2.20–2.40 (each 2H, m, 17-CH_2CH_2), 1.84 (3H, d, J = 7 Hz, 18-CH_3), 1.72 (3H, t, J = 8 Hz, 8^1-CH_3), 0.02, −1.94 (each 1H, s, NH); MS (FAB) (Found: M$^+$, 576. Calc. for $C_{35}H_{36}N_4O_4$: *M*, 576).

The above formylchlorin **11D** (10 mg) was reduced[21] by *t*-$BuNH_2$·BH_3 (20 mg) in dry CH_2Cl_2 (10 ml). Purification by FCC (0.75–1% CH_3OH–CH_2Cl_2) and recrystallization from CH_2Cl_2–hexane gave the corresponding 3-(3-hydroxyprop-1-enyl)chlorin **12D** (9.2 mg) in 92% yield; λ_{max}/nm (CH_2Cl_2) 667 (rel. 41%), 612 (7.4), 539 (8.7), 509 (10), 414 (100), 402 sh (84); ^{1}H-NMR ($CDCl_3$) δ 9.45, 9.29, 8.53 (each 1H, s, 5-, 10-, 20-H), 7.86 (1H, d, J = 16 Hz, 3-CH), 6.88 (1H, dt, J = 5, 16 Hz, 3^1-CH), 5.26, 5.10 (each 1H, d, J = 20 Hz, 13^1-CH_2), 4.75 (2H, d, J = 5 Hz, 3^2-CH_2), 4.47 (1H, dq, J = 2, 7 Hz, 18-H), 4.28 (1H, d, J = 8 Hz, 17-H), 3.64 (2H, q, J = 8 Hz, 8-CH_2), 3.65, 3.62, 3.38, 3.20 (each 3H, s, 2-, 7-, 12-CH_3, $COOCH_3$), 2.50–2.77, 2.20–2.40 (each 2H, m, 17-CH_2CH_2), 1.80 (3H, d, J = 7 Hz, 18-CH_3), 1.67 (3H, t, J = 8 Hz, 8^1-CH_3), 0.39, −1.75 (each 1H, s, NH); MS (FAB) (Found: M$^+$, 578. Calc. for $C_{35}H_{38}N_4O_4$: *M*, 578).

To a dry THF solution (10 ml) of the above chlorin **12D** (7 mg) was added PtO_2 (10 mg). After stirring of the mixture for 1.5 h under H_2 atmosphere, the PtO_2 was filtered off and the filtrate was washed with water three times and dried over Na_2SO_4. The solvents were evaporated off and the residue was

purified by FCC (1% CH_3OH–CH_2Cl_2) and recrystallized from CH_2Cl_2–hexane to give the 3-(3-hydroxypropyl)chlorin **12** (5.7 mg) in 81% yield; λ_{max}/nm (CH_2Cl_2) 657 (rel. 43%), 602 (7.7), 535 (8.6), 504 (9.0), 471 (3.6), 410 (100), 396 (77); ^{1}H-NMR ($CDCl_3$) δ 9.46, 9.27, 8.47 (each 1H, s, 5-, 10-, 20-H), 5.24, 5.09 (each 1H, d, J = 20 Hz, 13^1-CH_2), 4.45 (1H, dq, J = 2, 7 Hz, 18-H), 4.27 (1H, d, J = 8 Hz, 17-H), 3.85–3.98 (4H, m, 3-CH_2 + 3^2-CH_2), 3.68 (2H, q, J = 8 Hz, 8-CH_2), 3.65, 3.61, 3.30, 3.24 (each 3H, s, 2-, 7-, 12-CH_3, $COOCH_3$), 2.20–2.75 (6H, m, 3^1-CH_2 + 17-CH_2CH_2), 1.80 (3H, d, J = 7 Hz, 18-CH_2), 1.69 (3H, t, J = 8 Hz, 8^1-CH_3), 0.57, −1.63 (each 1H, s, NH); MS (FAB) (Found: *m/z* 581. Calc. for $C_{35}H_{41}N_4O_4$: MH^+, 581).

The above metal-free chlorin **12** was zinc-metallated[27], purified by FCC (1% CH_3OH–CH_2Cl_2) and recrystallized from CH_2Cl_2–hexane to give the title compound **3**; λ_{max}/nm (THF) 644 (rel. 77%), 599 (10), 564 (5.5), 519 (3.2), 423 (100), 403 (59); ^{1}H-NMR (10 v/v % CD_3OD–$CDCl_3$) δ 9.44, 9.06, 8.23 (each 1H, s, 5-, 10-, 20-H), 5.11, 4.97 (each 1H, d, J = 20 Hz, 13^1-CH_2), 4.37 (1H, dq, J = 2, 7 Hz, 18-H), 4.19 (1H, d, J = 8 Hz, 17-H), 3.60–3.90 (6H, m, 3-CH_2 + 3^2-CH_2 + 8-CH_2), 3.56, 3.42, 3.21, 3.16 (each 3H, s, 2-, 7-, 12-CH_3, $COOCH_3$), 2.20–2.77 (6H, m, 3^1-CH_2 + 17-CH_2CH_2), 1.75 (3H, d, J = 7 Hz, 18-CH_3), 1.67 (3H, t, J = 8 Hz, 8^1-CH_3); MS (FAB) (Found: M^+, 642. Calc. for $C_{35}H_{38}N_4O_4{}^{64}Zn$: *M*, 642).

Synthesis of zinc methyl 3^2-(hydroxymethyl)pyropheophorbide-*a* [3^1,3^2-didehydro-3^2-(hydroxymethyl)phytochlorinatozinc(II) methyl ester 3D]

Metal-free chlorin **12D** was zinc-metallated,[27] purified by FCC (1% CH_3OH–CH_2Cl_2) and recrystallized from CH_2Cl_2–hexane to give **3**; λ_{max}/nm (THF) 654 (rel. 66%), 608 (11), 568 (5.6), 522 (3.8), 427 (100), 407 (78); ^{1}H-NMR (10 v/v % CD_3OD–$CDCl_3$) δ 9.49, 9.22, 8.34 (each 1H, s, 5-, 10-, 20-H), 7.84 (1H, d, J = 16 Hz, 3-CH), 6.76 (1H, dt, J = 5, 16 Hz, 3^1-CH), 5.15, 5.02 (each 1H, d, J = 20 Hz, 13^1-CH_2), 4.67 (2H, d, J = 5 Hz, 3^2-CH_2), 4.41 (1H, dq, J = 2, 7 Hz, 18-H), 4.22 (1H, d, J = 7 Hz, 17-H), 3.72 (2H, q, J = 8 Hz, 8-CH_2), 3.60, 3.40, 3.30, 3.23 (each 3H, s, 2-, 7-, 12-CH_3, $COOCH_3$), 2.20–2.65 (4H, m, 17-CH_2CH_2), 1.76 (3H, d, J = 7 Hz, 18-CH_3), 1.69 (3H, t, J = 8 Hz, 8^1-CH_3); MS (FAB) (Found: M^+, 640. Calc. for $C_{35}H_{36}N_4O_4{}^{64}Zn$: *M*, 640).

Acknowledgements

We thank Drs Tadashi Mizoguchi, Yoshitaka Saga and Luke Ueda-Sarson of Ritsumeikan University for helpful discussions. S. Y. thanks the Japan Science Society for a Sasakawa Scientific Research Grant.

References

1 J.-M. Lehn, *Supramolecular Chemistry. Concepts and Perspectives*, VCH, Weinheim, 1995.
2 H. Tamiaki, *Coord. Chem. Rev.*, 1996, **148**, 183.
3 J. M. Olson, *Photochem. Photobiol.*, 1998, **67**, 61.
4 G. McDermott, S. M. Prince, A. A. Freer, A. M. Hawthornthwaite-Lawless, M. Z. Papiz, R. J. Cogdell and N. W. Isaacs, *Nature (London)*, 1995, **374**, 517.
5 P. Jordan, P. Fromme, H. T. Witt, O. Klukas, W. Saenger and N. Krauβ, *Nature (London)*, 2001, **411**, 909.
6 P. Hildebrandt, H. Tamiaki, A. R. Holzwarth and K. Schaffner, *J. Phys. Chem.*, 1994, **98**, 2192.
7 A. R. Holzwarth and K. Schaffner, *Photosynth. Res.*, 1994, **41**, 225.
8 H. Tamiaki, M. Amakawa, Y. Shimono, R. Tanikaga, A. R. Holzwarth and K. Schaffner, *Photochem. Photobiol.*, 1996, **63**, 92.
9 H. Tamiaki, T. Miyatake, R. Tanikaga, A. R. Holzwarth and K. Schaffner, *Angew. Chem., Int. Ed. Engl.*, 1996, **35**, 772.
10 T. Miyatake, H. Tamiaki, A. R. Holzwarth and K. Schaffner, *Photochem. Photobiol.*, 1999, **69**, 448.
11 T. Miyatake, H. Tamiaki, A. R. Holzwarth and K. Schaffner, *Helv. Chim. Acta*, 1999, **82**, 797.
12 K. M. Smith, D. A. Goff and D. J. Simpson, *J. Am. Chem. Soc.*, 1985, **107**, 4946.
13 R. K. Pandey, N. Jagerovic, J. M. Ryan, T. J. Dougherty and K. M. Smith, *Tetrahedron*, 1996, **52**, 5349.
14 H. Tamiaki, T. Watanabe and T. Miyatake, *J. Porphyrins Phthalocyanines*, 1999, **3**, 45.
15 R. J. Abraham, A. E. Rowan, N. W. Smith and K. M. Smith, *J. Chem. Soc., Perkin Trans. 2*, 1993, 1047.
16 H. Tamiaki and M. Kouraba, *Tetrahedron*, 1997, **53**, 10677.
17 B. E. Maryanoff, A. B. Reitz and B. A. Duhl-Emswiler, *J. Am. Chem. Soc.*, 1985, **107**, 217.
18 B. Fraser-Reid, B. F. Molino, L. Magdzinski and D. R. Mootoo, *J. Org. Chem.*, 1987, **52**, 4505.
19 S. Yagai, T. Miyatake, Y. Shimono and H. Tamiaki, *Photochem. Photobiol.*, 2001, **73**, 153.
20 C.-J. Li, *Tetrahedron*, 1996, **52**, 5643.
21 S. Yagai, T. Miyatake and H. Tamiaki, *J. Photochem. Photobiol. B: Biol.*, 1999, **52**, 74.
22 D. R. Buck and W. S. Struve, *Photosynth. Res.*, 1996, **48**, 367.
23 H. Tamiaki, M. Amakawa, A. R. Holzwarth and K. Schaffner, *Photosynth. Res.*, in press.
24 R. G. Alden, S. H. Lin and R. E. Blankenship, *J. Lumin*, 1992, **51**, 51.
25 H. Tamiaki, S. Miyata, Y. Kureishi and R. Tanikaga, *Tetrahedron*, 1996, **52**, 12421.
26 Y. Saga, K. Matsuura and H. Tamiaki, *Photochem. Photobiol.*, 2001, **74**, 72.
27 H. Tamiaki, S. Yagai and T. Miyatake, *Bioorg. Med. Chem.*, 1998, **6**, 2171.